Engineering Structures 220 (2020) 110977

Contents lists available at ScienceDirect

Engineering Structures

journal homepage: www.elsevier.com/locate/engstruct

System-level modeling methodology for capturing the pile cap, helical pile group, and soil interaction under uplift loads

Anish Sharma*, Serhan Guner

Department of Civil and Environmental Engineering, University of Toledo, Toledo, OH 43607, USA

ARTICLE INFO

Keywords:
Axial load
Concrete modeling
Experimental benchmark
Methodology
Model calibration
Nonlinear response
Pile cap
Soil
Soil-structure interaction
Tension

ABSTRACT

In tall and light structures, such as transmission towers, wind turbines, and light-gauge steel structures, there is an increasing application of pile cap with helical pile foundation systems to resist the uplift loads due to the effects of windstorms and earthquakes. There is a lack of knowledge, published literature, or analysis methods to account for the effects of the pile cap, helical pile group, and soil interactions on the holistic response of the foundations, particularly, for the load conditions creating net uplift loads. In the lack of such, discrete modeling approaches are frequently employed in practice. These approaches isolate each system component and analyze them individually, neglecting the interactions between them. In an attempt to bridge this knowledge gap, this study proposes a system-level modeling methodology for the holistic analysis of pile cap systems in dry soil and static load conditions, while accounting for the effects of interactions between system components and the inherent material nonlinearities. The methodology employs a three-stage process in which the material and interaction properties are calibrated with the experimental benchmark specimens. The failure mechanisms are also experimentally verified based on the relative displacement of the piles. Important modeling considerations are discussed, and experimental benchmark specimens are provided to assist practitioners in accurately performing system-level analyses. The effectiveness of the proposed methodology is discussed, and the responses obtained, including the load–displacement responses, load capacities, and failure modes, are compared with those obtained from the discrete modeling approaches. The results demonstrate that discrete modeling approaches significantly underestimate the load capacity while not accurately predicting the governing behavior and the failure modes.

1. Introduction

The design of tall and light structures, such as latticed towers (supporting telecommunication equipment or transmission lines), wind turbines, and light-gauge steel frame structures, are typically governed by the large overturning moments generated by lateral loads. These moments create tension–compression force couples and may expose windward side foundations to significant net uplift forces, which are typically more challenging to resist than the compression loads. Helical piles are increasingly more commonly used in practice to resist the uplift effects of the lateral loads due to their high tensile capacities, low disturbance to surroundings, and suitability to construction sites with limited access or space [1,2]. Helical piles are typically installed in groups and connected to a pile cap or a pile cap strip (e.g., a grade beam) to create two- or one-way stress flows. A successful design of a helical pile foundation system requires accurately capturing the responses of the pile cap, pile group, soil, and the interactions between them [3-9]. There is, unfortunately, a lack of knowledge and analysis methods in the literature to account for these effects holistically when resisting uplift loads. Analysis of helical foundation systems is predominantly conducted in practice using discrete modeling approaches performed by structural and geotechnical engineers separately. In this approach, the structural analysis focuses on the isolated pile cap [10-12] and neglects the effects of the piles and soil by assuming pile shafts pinned or fixed (e.g., Fig. 1a). The main focus of the structural analysis is to design the concrete foundation and obtain the pile end reactions (i.e., the forces applied to piles). The geotechnical analysis, on the other hand, uses these reactions and models the soil and the helical piles explicitly [13-15] while the effects of the pile cap, including pile to pile cap connections, are neglected (e.g., Fig. 1b). There is a need to establish a system-level modeling methodology (e.g., Fig. 1c) to overcome the current challenges and asses the consequences of using the currently

* Corresponding author.
E-mail addresses: anish.sharma@rockets.utoledo.edu (A. Sharma), serhan.guner@utoledo.edu (S. Guner).

https://doi.org/10.1016/j.engstruct.2020.110977
Received 10 December 2019; Received in revised form 7 May 2020; Accepted 15 June 2020

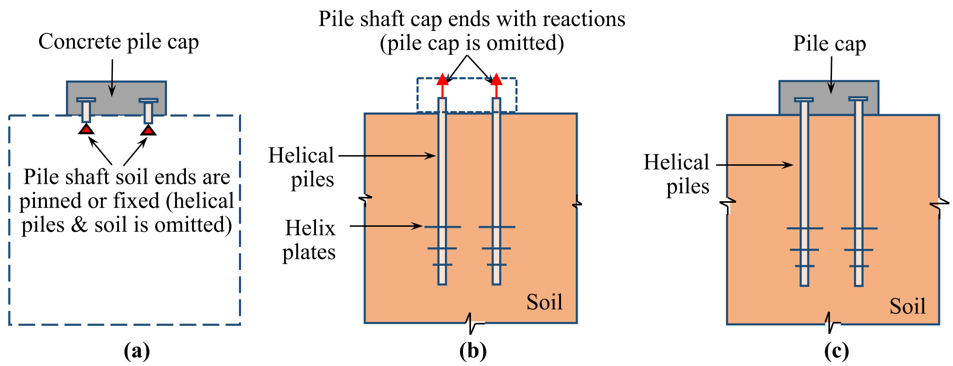

Fig. 1. Modeling approaches: (a) discrete foundation model (i.e., structural modeling), (b) discrete helical piles and soil model (i.e., geotechnical modeling), and (c) the proposed system-level model.

employed discrete modeling approaches.

The current advancement in the computational capabilities of high-fidelity nonlinear finite element (NLFE) modeling has proven to be a versatile tool for studying the behavior and the interactions between structural and geotechnical components [16-19]. As compared to other methods such as the finite difference method, NLFE modeling provides advantages for the simulation of the holistic response of the foundations, including the concrete and connection modeling. In addition, NLFE is more flexible for the analysis of complex geometrical problems with several interactions between system components [20,21]. Several studies employing NLFE modeling have attempted to predict the soil response using theories such as the Mohr-Coulomb [22], Drucker-Prager [23] or Modified Drucker-Prager [24] while employing contact elements with interactions defined by friction factors between the concrete, steel, and soil [25-29]. Past studies proposed modeling approaches for common types of pile foundation – such as circular or prismatic concrete piles – subjected to tensile uplift load conditions (e.g., [30-33]). Fewer studies investigated the helical piles and soil under uplift loads [4,34-36]. Some of these studies employed two-dimensional (2D) finite element models [26,27] while more recent studies presented three-dimensional (3D) finite element models [29,34,35]. These studies, however, did not attempt to generalize or propose a methodology for the modeling of helical piles; rather, they presented models created and calibrated to meet case-specific applications (i.e., usually a few experimental tests).

This paper presents a 3D system-level modeling methodology for helical pile foundation systems. The methodology can be applied to evaluate the static response of foundations, including static-equivalent forces from dynamic excitations such as earthquakes or windstorms, in dry soils while accounting for material nonlinearities, and the effects of pile cap, helical pile group, and soil interactions. The proposed methodology does not require the use of specific computer software because it calibrates the material and interaction properties with experimental benchmarks studies from the literature, which are also presented in this paper to assist researchers and practitioners in employing the proposed methodology. The methodology uses an experimentally verified failure mechanism of the helical pile foundation system based on the relative displacement of the helical piles. The traditional, discrete modeling approaches are also employed to demonstrate how the response predictions compare with the proposed system-level modeling methodology in terms of the load–displacement responses, load capacities, and failure modes. In addition, numerical studies are performed to demonstrate the influences of critical parameters such as the soil conditions, embedment depth of the helical piles inside the concrete foundation and the soil, and the number of helix plates. While a special emphasis is placed on the load conditions creating net uplift loads, the applicability of the methodology to more traditional compression load cases are also presented.

2. Proposed system-level modeling methodology

The proposed methodology employs three main stages as summarized in Fig. 2. These stages include: 1) verification of the behavior of the discrete pile cap model, 2) verification of the behavior of the discrete helical pile group and soil model, and 3) system-level modeling. The goal is to obtain the experimentally calibrated material and interaction models in Stages 1 and 2 using experimental benchmark studies (to be presented below) such that an experimentally verified system-level model could be created in Stage 3.

2.1. Verification of the behavior of discrete pile cap model

The first stage of the proposed methodology requires the creation of a NLFE model for the discrete pile cap. Any NLFE modeling software can be used, on the condition that it has capabilities for simulating the expected nonlinear behaviors of materials and interaction properties after the calibration studies presented below. In this study, the concrete damage plasticity (CDP) model, which is based on scalar plastic damage models proposed by Lee and Fenves [37], and Lubliner [38], is employed as a constitutive model to simulate the nonlinear response of concrete (see Fig. 3a). The CDP model can also simulate the effects of the interactions between the concrete and reinforcing bars. Reinforcing bars are modeled as an elastic–plastic material, with the stress–strain response shown in Fig. 3b.

These material models were previously used in other studies to capture significant failure modes, including punching shear (see Fig. 4a), one-way shear (see Fig. 4b), and flexural failures (see Fig. 4c) [39,40].

After the material behaviors are defined, boundary conditions are applied at the support ends of the foundation. If a symmetrical model is created, rollers should also be defined along the axis of symmetry. A pushover analysis is performed up to the failure of the foundation using a displacement-controlled loading protocol which permits the analysis to continue into the post-peak stages of the response, thereby showing the ductility and hardening or softening behavior of the foundation. At the end, the load–displacement response is obtained. To verify the NLFE load–displacement response, experimental benchmark studies are conducted to assess the accuracy in terms of the initial stiffnesses, ultimate load capacities, and the failure modes. In the case of a discrepancy (e.g., larger than ± 10%), the material models and/or their required input properties (see Fig. 3) should be adjusted, and the process is repeated until an adequate accuracy is obtained.

2.1.1. Experimental benchmarks for discrete pile cap model

A number of suitable experimental benchmark specimens are identified from the literature, which can be used for the calibration of the NLFE material models when employing the proposed methodology. The specimens are selected to exhibit predominantly shear and shear-

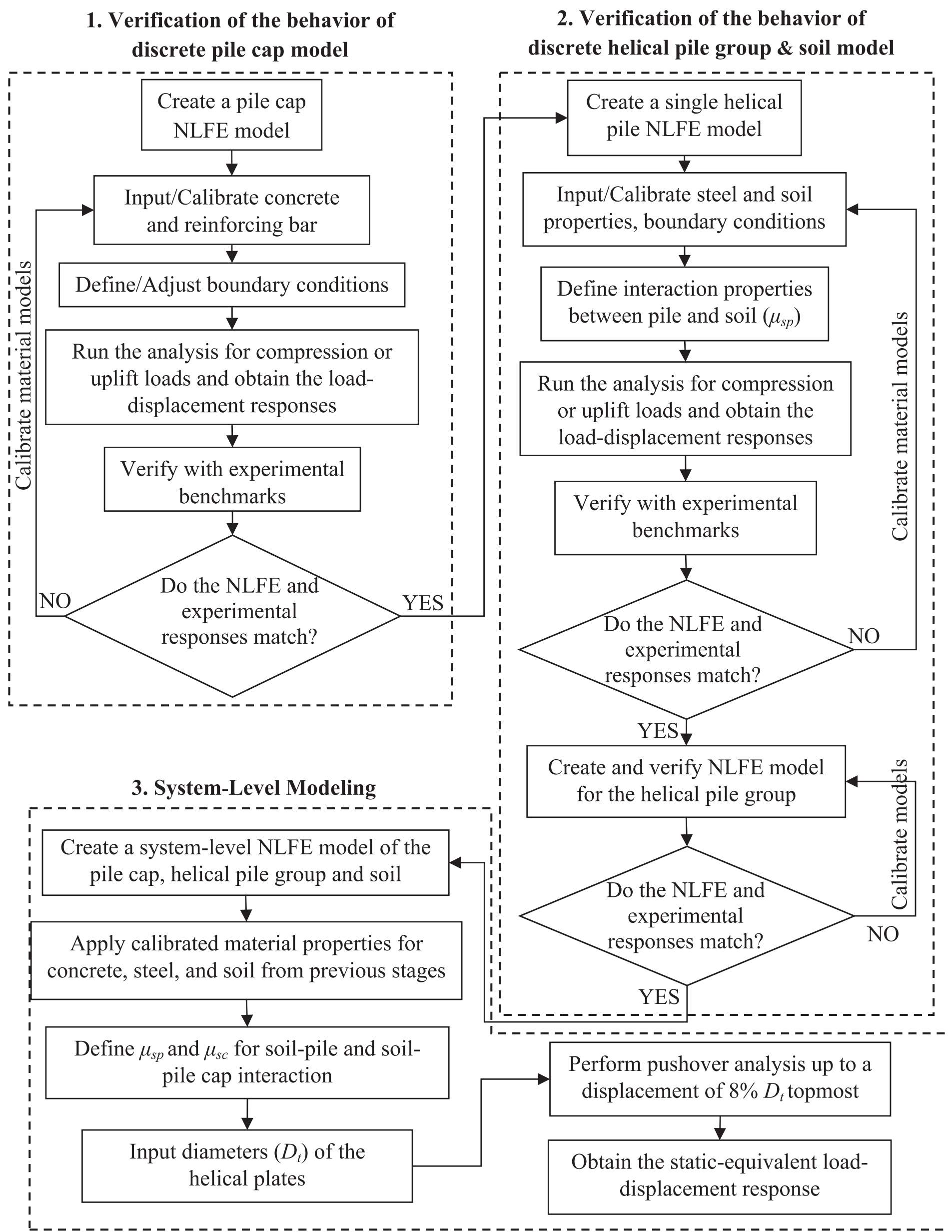

Fig. 2. Flowchart of the proposed system-level modeling methodology.

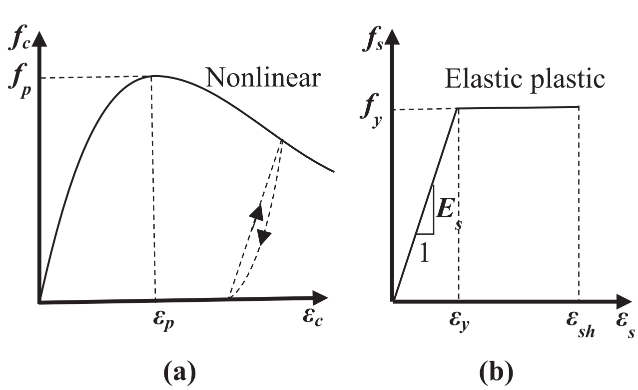

Fig. 3. Constitutive models for (a) concrete, and (b) reinforcing bar.

compression types of failures because most foundations are deep concrete elements and exhibit these types of failures, and they are more challenging to capture as compared to reinforcing-steel-governed flexural failures. Both the compression and uplift load conditions are considered.

For the compression loading, the NLFE response can be verified with the experimental specimens tested by Vecchio and Shim [41]. This benchmark set includes twelve simply supported beam strips of height 552 mm with different lengths and design configurations subjected to monotonically increasing compression loads at their midspans. Test results including the load–displacement responses, load capacities, and failure modes are reported in detail in reference [41]. The cross-sectional details, material properties, failure loads (P_u), and failure displacements (δ_u) are presented in Table 1.

For the load cases involving net uplift loading, the NLFE response

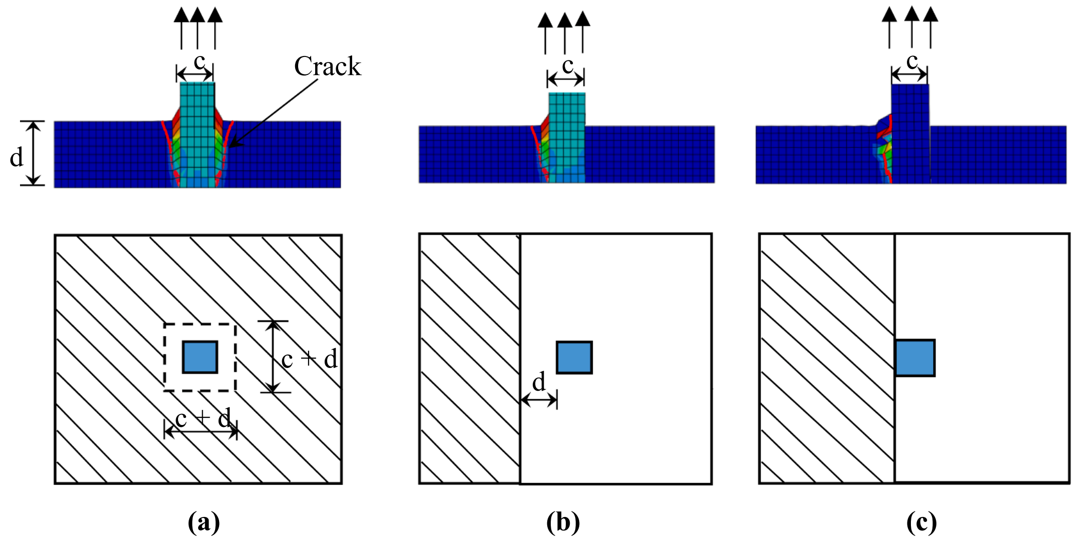

Fig. 4. Global failure modes of a discrete pile cap: (a) punching shear, (b) one-way shear, and (c) flexure.

Table 1
Experimental benchmark set for discrete foundation modeling under compression [41].

Beam number	Length (mm)	Width (mm)	f'_c (MPa)	E_c (MPa)	Bottom rebar	Top rebar	Stirrups	P_u (kN)	δ_u (mm)
VS-OA1	4100	305	22.6	36,500	2 M30, 2 M25	–	–	331	9.1
VS-OA2	5010	305	25.9	32,900	3 M30, 2 M25	–	–	320	13.2
VS-OA3	6840	305	43.5	34,300	4 M30, 2 M25	–	–	385	32.4
VS-A1	4100	305	22.6	36,500	2 M30, 2 M25	3 M10	D5 @ 210	459	18.8
VS-A2	5010	305	25.9	32,900	3 M30, 2 M25	3 M10	D5 @ 210	439	29.1
VS-A3	6840	305	43.5	34,300	4 M30, 2 M25	3 M10	D4 @ 168	420	51.0
VS-B1	4100	229	22.6	36,500	2 M30, 2 M25	3 M10	D5 @ 190	434	22.0
VS-B2	5010	229	25.9	32,900	3 M30, 2 M25	3 M10	D5 @ 190	365	31.6
VS-B3	6840	229	43.5	34,300	3 M30, 2 M25	3 M10	D4 @ 152	342	59.6
VS-C1	4100	152	22.6	36,500	2 M30	3 M10	D5 @ 210	282	21.0
VS-C2	5010	152	25.9	32,900	2 M30, 2 M25	3 M10	D5 @ 210	290	25.7
VS-C3	6840	152	43.5	34,300	2 M30, 2 M25	3 M10	D4 @ 168	265	44.3

Sectional areas: M10 = 100 mm^2; M25 = 500 mm^2; M30 = 700 mm^2; D4 = 25.7 mm^2; D5 = 32.2 mm^2.

Table 2
Experimental benchmark set for discrete foundation modeling under uplift [42]

Specimen	f'_c (MPa)	Top & bottom rebars	Stirrups	d_e (mm)	P_u (kN)	δ_u (mm)
T1	30	4–15 M	2-#2 @ 200	152	154.0	2.5
T2	30	4–15 M	2-#2 @ 200	203	201.0	3.6
T3	30	4–15 M	2-#2 @ 200	254	232.0	2.0
T4	40	4–20 M	2-#2 @ 200	203	222.5	1.3
T5	40	4–25 M	2-#2 @ 200	203	252.3	1.0
T6	40	4–15 M	4-#2 @ 200	203	256.3	6.4
T7	40	4–15 M	2-#2 @ 200	203	253.2	2.7

Sectional areas: M15 = 200 mm^2; M20 = 300 mm^2; M25 = 500 mm^2; #2 = 32 mm^2.

can be calibrated with the experimental specimens tested by Diab [42]. This benchmark set includes seven discrete pile cap strips of dimensions 500 × 500 × 1600 mm subjected to uplift loading. The test results, including the load–displacement responses, load capacities, and failure modes, are reported in detail in Ref. [42]. The uplift loading is applied by pulling the specimens from the embedded pile shafts with varying embedment depths (d_e). The material properties, failure load (P_u), and failure displacement (δ_u) are shown in Table 2. The calibrated material model parameters that yield acceptable response simulations with the experimental benchmark sets are recorded for use in Stage 3 when creating a system-level model.

2.2. *Verification of the behavior of the discrete helical pile group and soil model*

The second stage of the proposed methodology requires the creation of a NLFE model for the discrete helical pile group and soil model through a two-step process involving a single helical pile, and a group of helical piles. The single helical pile, made up of steel material, is modeled with an elastic–plastic constitutive model as shown in Fig. 3b. The soil is modeled with an elastoplastic constitutive model with a failure mode governed by the Mohr-Coulomb criterion [43]. While this model has limitations [44-46], it has been shown to yield satisfactory results from granular to cohesive, fine-grained soils under both drained and undrained load conditions (e.g., [19,32,33,47]). In this study, the presence of water in the soil continuum is not modeled, and a dry soil condition is considered. If the shear stress (τ) is greater than $c + \sigma$ tan

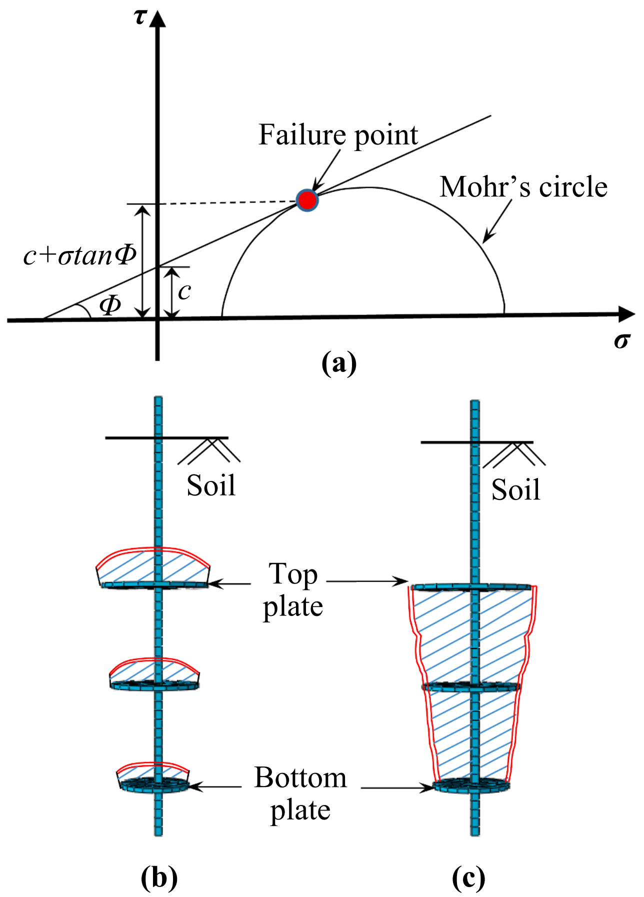

Fig. 5. Discrete helical pile model: (a) soil constitutive model, (b) individual plate bearing failure, and (c) cylindrical shear failure.

Table 3
Interface properties of different materials [49].

Interface materials		Friction factor	Friction angle
Concrete	Rock	0.70	35
	Gravel	0.55–0.60	29–31
	Medium sand	0.35–0.45	19–24
	Stiff clay	0.30–0.35	17–19
Steel	Gravel	0.40	22
	Silty sand	0.25	14
	Fine sandy slit	0.20	11

Φ, where c is the cohesion, Φ is the friction angle of soil, and σ is the normal stress, the soil fails as per Fig. 5a. This failure criterion is used for its simplicity and applicability for simulating the soil-structure interaction as demonstrated in other studies (e.g., [43]). Two independent material parameters (Young's modulus E, and Poisson's ratio ν) are also required as input. This material model, which can easily be applied to commercial software packages, can simulate the two primary failure modes: individual plate uplift bearing where the failure occurs above each individual helix plate (see Fig. 5b), and cylindrical shear where a global failure is formed through the plate and the soil acting together to create a cylinder failure surface (see Fig. 5c). Individual plate uplift bearing occurs when helical piles are installed in dense homogeneous cohesionless soil whereas the cylindrical shear occurs

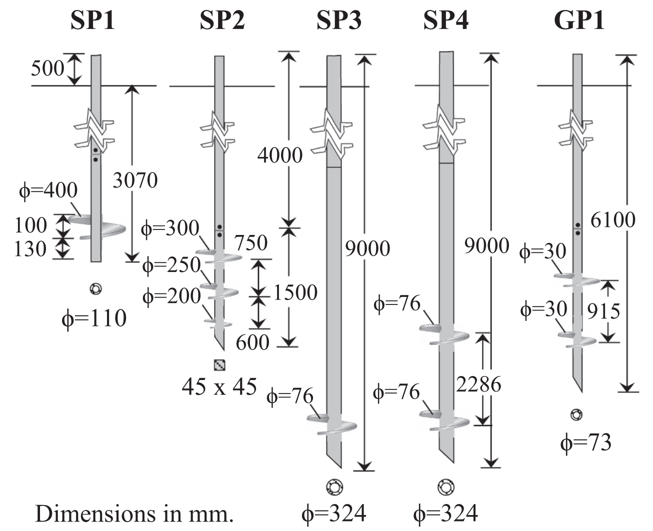

Fig. 6. Geometrical details of the benchmark pile specimens.

Table 4
Soil properties for the benchmark pile specimens.

Specimen	E (MPa)	Φ (°)	ψ (°)	c (kPa)	Soil Type (USCS)
SP1	23	56	33	0	GW
SP2	54	28	0	10	OL
SP3	48	35	5	1	GM-GL
SP4	48	35	5	1	GM-GL
GP1	50	22*	0	25	CH

* Estimated based on USCS soil classification [54].

when helical piles are installed in homogeneous cohesive soil (e.g., [19]). The spacing between the helix plates also influences the failure mode experienced by the helical pile, where spacings lower than 3–4 helix plate diameters are found to cause cylindrical shear failures [48].

The main objective of Stage 2 is to obtain the experimentally calibrated interaction model to simulate the interface between the soil and the piles. The typical soil deformations that occur in soil-pile interactions include plastic flow and expansion (i.e., dilation), which can occur with shear deformation, soil compaction, and soil distortion. These interactions in the interface between the pile cap, helical piles, and the soil depend on the friction angle and adhesion. For deep helical piles, the contribution of the friction along the pile shaft may be considered. The interaction behavior between soil and pile is typically defined by an experimentally determined coefficient of friction. The friction between the two surfaces in contact depends on the material properties of the surfaces. In the absence of experimental results, common soil-structure friction factors from NAVFAC standards [49] may be used, as presented in Table 3. While some studies (e.g., [34]) suggested a reduction in the friction factors shown in Table 3 to account for uplift loads, other studies (e.g., [35]) were able to validate helical pile models under uplift loads without friction factor changes. For the helical pile foundation system investigated in this study (to be discussed in Section 3), reducing the friction factor did not result in a significant change in system-level response.

A displacement-controlled axial loading is applied at the top of the helical piles while the helix plate displacements are recorded. The load–displacement response is obtained for verification with the

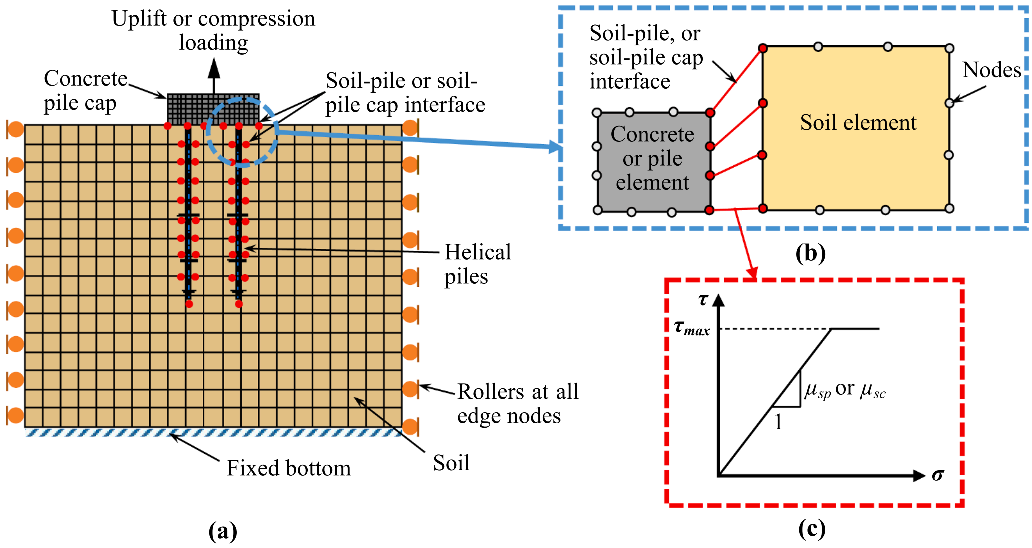

Fig. 7. (a) A sample system-level model, (b) interface model, and (c) interaction model at the interfaces.

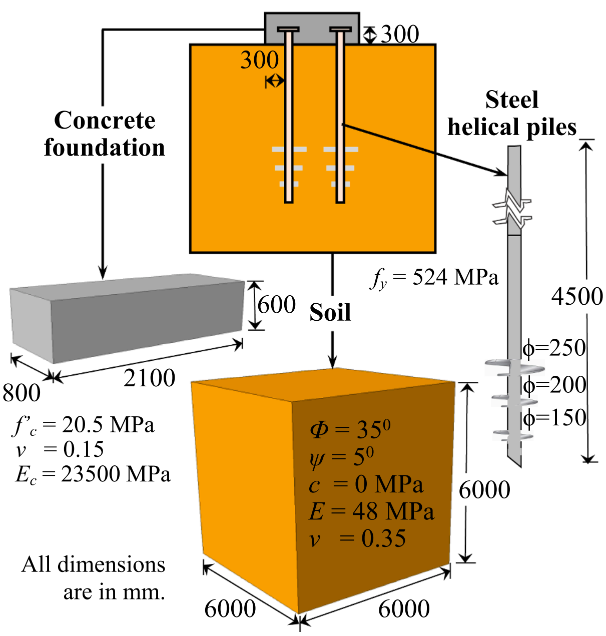

Fig. 8. Details of the system investigated.

experimental benchmark studies to assess the accuracy in terms of the initial stiffness, the ultimate capacity and displacement, and the failure mode. In the case of a discrepancy (e.g., larger than ± 10%), the soil input material and interaction properties are adjusted, and the process is repeated until an adequate accuracy is obtained. Depending on the degree of confidence in the soil properties used in the model, certain combinations of the required material properties (i.e., E, ν, c, Φ) may need to be adjusted. In addition, the interaction friction factor between the soil and helical piles may require adjustment, as this interaction property is the source of extensive debate in the literature (e.g., [19,32,47]).

For helical pile groups, past research revealed that no significant group interactions should occur if the piles are placed at a horizontal distance of at least three and five times the diameter of the largest helix plate for compression and uplift load conditions, respectively [35,50]. If these distance limits are satisfied, only the verification of the single helical pile response is necessary; otherwise, a model of the helical pile group should be created and verified in a similar manner.

2.2.1. Experimental benchmarks for single and grouped helical pile-soil model

A number of suitable experimental benchmark specimens are selected from the literature and can be used for the calibration of the NLFE model when employing the proposed methodology. The geometric details and the soil properties are presented in Fig. 6 and Table 4, respectively. For the single pile model, the NLFE response can be verified with four experimental specimens (SP1, SP2, SP3, and SP4) tested by Gavin et al. [51], Sakr [52], and Livneh and Naggar [35]. For the helical pile group model, the NLFE response can be verified with the 2 × 2 experimental helical pile specimens (GP1) tested by Lanyi and Deng [53]. These specimens are selected to exhibit predominantly cylindrical shear failures common in helical pile foundations. Test results, including load–displacement responses, load capacities, and failure modes, are reported in detail in references [35,51-53]. The properties of the soil are provided and classified by the united soil classification system (USCS) standards [54]. The available data is sufficient to model the soil using the Mohr-Coulomb criterion [43], as discussed previously.

2.3. Establishing the system-level model

The system-level model of the helical pile foundation systems is created based on the experimentally calibrated material and interaction models obtained from Stages 1 and 2. When creating a system-level model (e.g., Fig. 7a), the main consideration should be given to how the interface is defined between the soil and pile cap (denoted with subscript sc) and soil and helical piles (denoted with subscript sp). In this study, these interfaces are defined by pairing contact elements as shown in Fig. 7b. This interaction model is based on the Coulomb law of friction [22,43] which relies on the coefficient of friction (μ_{sc} or μ_{sp})

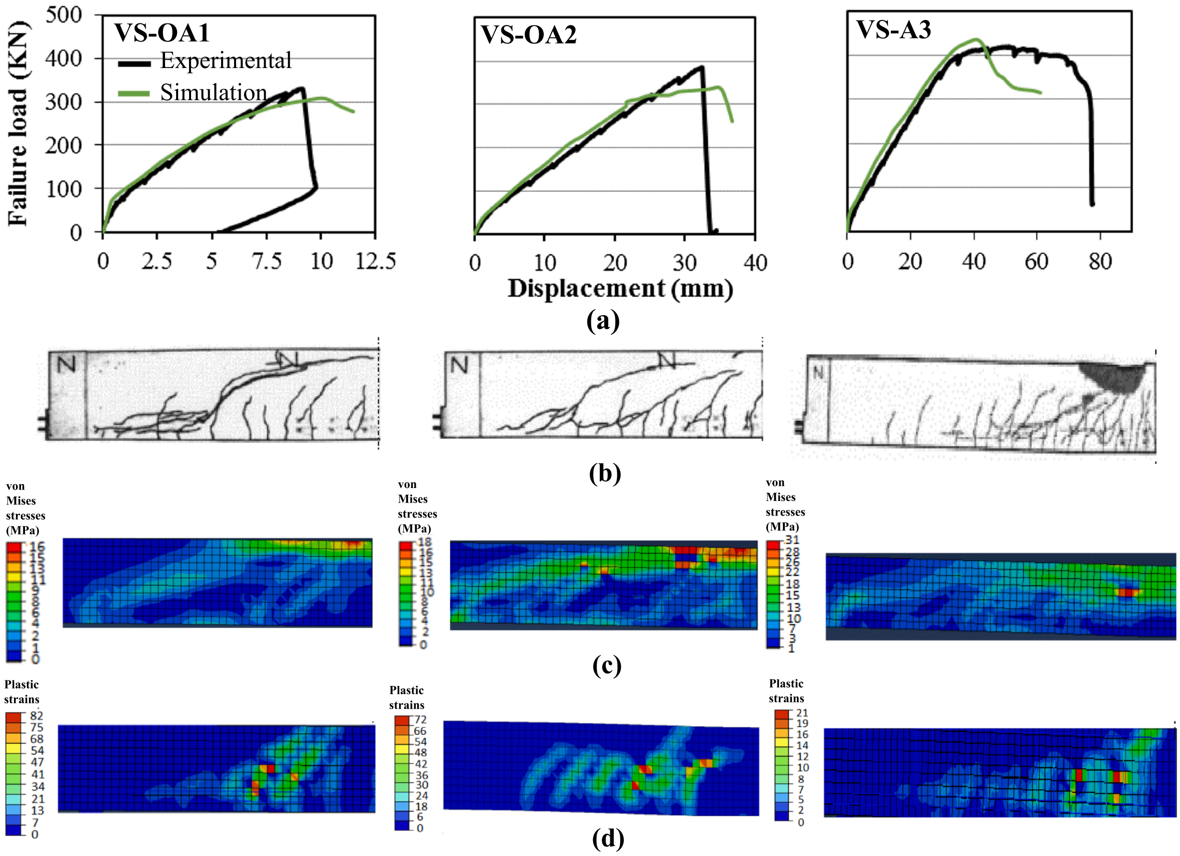

Fig. 9. (a) Load-displacement responses, (b) experimental crack patterns at failure [41], (c) predicted stresses distributions, and (d) predicted crack patterns under compression load.

Table 5
. Input parameters for concrete under compression.

Parameter	Value
Dilation angle (ψ)	35
Eccentricity (ϵ)	0.1
fb_o/fc_o	1.16
K	0.667
Viscosity (μ)	0.0001

between two surfaces in contact (see Fig. 7c). The interface between the helical pile termination brackets and the pile cap is considered to be perfectly bonded to the surrounding concrete given that it is a cast-in-place connection.

When defining the boundary conditions, special attention should be paid to ensure that the variations in the strain gradient are contained within the modeled soil area to ensure that the model of the soil mass is sufficiently large. Prior to the application of the load, the soil unit weight is accounted for in the numerical model as an initial stress through a geostatic equilibrium. In this pre-loading stage, the boundaries on the bottom and sides of the soil continuum are fixed and the gravitational acceleration is applied [55]. The lateral earth pressure resulting from the vertical stresses are calculated using Eq. (1), where σ_h is the horizontal stress and σ_v is the vertical stress. For practical purposes, the value of K is considered as 1.0 [56]. The stable state of the system-level model under gravity loads is obtained and the stresses calculated by this step are used as the initial loading state for the analysis. Helical piles cause little disturbance to the surrounding soil; therefore, the effects of pile installation method, including the shear strength modification, are not considered in this study. In the case of employing square shafts in cohesive soils, however, these modifications may help improve the prediction accuracy.

$$K = \frac{\sigma_h}{\sigma_v} \tag{1}$$

A displacement-controlled loading is desired, as opposed to a force-controlled one, at the top of the concrete pile cap (see Fig. 7a) in a monotonically increasing manner until the failure. Displacement control will allow the analysis to continue in the post-peak region allowing the quantification of the deformation capacity of the system and more accurate identification of the failure mode. The Mohr-Coulomb failure criterion with an 8% displacement cut-off (i.e., 8% of the topmost helix plate diameter, D_t) is found to successfully capture the experimental responses considered in this study. Similar failure criterion ranging from 5% to 10% of the lead helix diameter are also found suitable in other studies (e.g., [19,35]). At the end of the analysis, a system-level load–displacement response is obtained from which the stiffness, peak load capacity, and the displacement ductility can be obtained. The failure mode of the system should be carefully determined after examining the deformed shape, stress and strain contours, and the post-peak stages of the load displacement response.

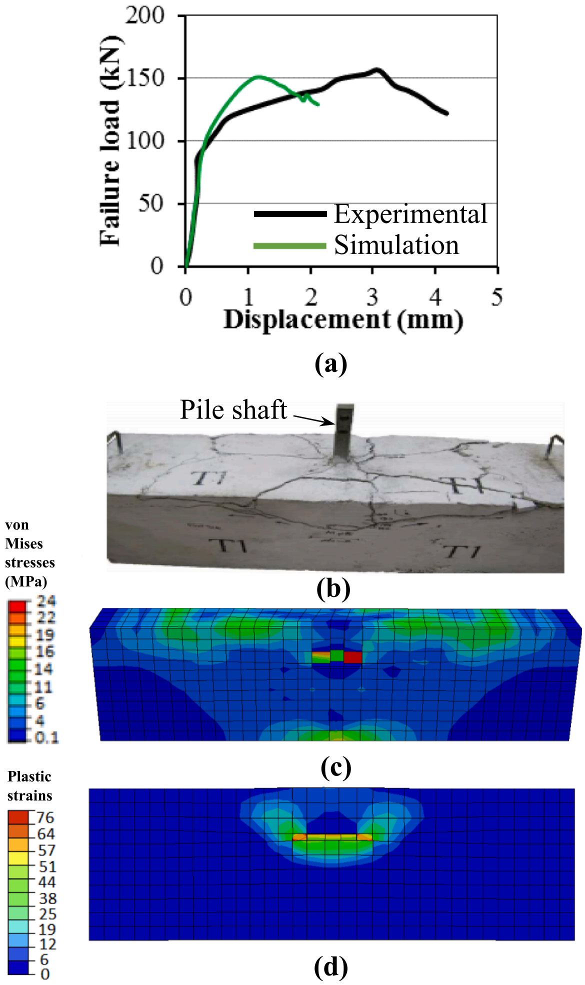

Fig. 10. (a) Load-displacement response, (b) experimental crack patterns [42], (c) stress distribution, and (d) plastic strains from the FE simulation under tension load.

Table 6
Input parameters for concrete under tension.

Parameter	Value
Dilation angle (ψ)	37
Eccentricity ($\in$)	0.1
fb_o/fc_o	1.16
K	0.667
Viscosity (μ)	0.0001

3. Application of the system-level modeling methodology

In this section, numerical studies are presented to illustrate the application of the proposed methodology for performing system-level modeling of a helical pile foundation system embedded in silty sand (i.e. 50% of the coarse fraction passing the 4.75 mm sieve). The geometric and material details of discrete components (i.e. concrete foundation, steel helical pile, and the soil) of the system to be modeled is shown in Fig. 8.

The proposed methodology requires that a discrete concrete foundation model is created and experimentally verified first. While the program Abaqus [57] is used in this study, any other NLFE modeling program can be used, on the condition that it can capture the primary behaviors expected from the system being modeled. The pile cap is discretized with eight-node, first-order, and reduced integration continuum solid element C3D8R with three translational degrees of freedom at each node and one integration point at the centroid. The reinforcement bars are discretized with two-node, first-order, 3D truss element T3D2 with three translational degrees of freedom at each node and one integration point at the mid-length of the elements. In Stage 1, the material properties, interaction properties, and boundary conditions for concrete pile cap model are defined as discussed in Section 2. The model calibration process is performed herein for both compression and uplift loads for demonstration purposes. The compression load verification is conducted using the experimental benchmarks VS-OA1, VS-OA2, and VS-A3 subjected to mid-span displacements. The complete load–displacement responses (see Fig. 9a) and the failure modes (see Fig. 9b, c, and d) are obtained and compared with the experimental results. The von Mises stresses are used to visualize how stresses are distributed within the discrete pile cap, identify if the material yields or fractures, and consistently compare with the stresses obtained in the rest of this study. It should be noted that the use of von Mises stresses is not recommended for brittle materials like concrete. The strain gradients are used to visualize the damage patterns; as such, the plastic strain contours in the concrete model are compared with the experimental cracking patterns for validation purposes. At the end, the discrepancy between the FE simulation and experimental values of the peak load capacities are found to be less than 10%, indicating a successful calibration for the material model parameters shown in Table 5, where fb_o/fc_o is the ratio of the initial biaxial compressive yield stress to the initial uniaxial compressive yield stress, and K is the ratio of the second stress invariant on the tensile meridian to that on the compressive meridian. It should be noted that the benchmark specimens should be carefully selected to incorporate the expected behaviors. The specimens VS-OA1 and VS-OA2 used in this study contained no shear stirrups, similar to the pile cap modeled, and failed in diagonal-tension and shear-dominated failure modes.

A similar process is employed for the uplift load case using the benchmark Specimen FT1 (see Table 2). The results of the experimental verification study are presented in Fig. 10 in terms of the load–displacement response and failure modes. The calibrated material model input is presented in Table 6.

In Stage 2, a discrete helical pile group and soil model is created (see Fig. 11a) through a two-step process. The first step involves experimentally verifying a single helical pile model while the second step involves verifying the helical pile group model (incorporating the calibrated single pile models) to obtain the calibrated material and interaction properties. For the first step, the material properties and boundary conditions are defined as discussed in Section 2. The C3D8R continuum solid element is used to discretize the helical piles and the soil medium. The helix plates of each helical pile are idealized as a planar cylindrical disk, as opposed to a pitched geometry, which is a simplifying approach validated in several other studies (e.g., [19,26,58]). To model the interaction between soil and helical pile, the master-and-slave surface approach with hard contact is adopted, which is defined with the coefficient of friction obtained from Table 3. Pushover analyses are performed to obtain the load–displacement responses for comparison with the experimental results. For the second step, a benchmark helical pile group system model (i.e., GP1 in Fig. 6) is created and the material models are calibrated, following a similar

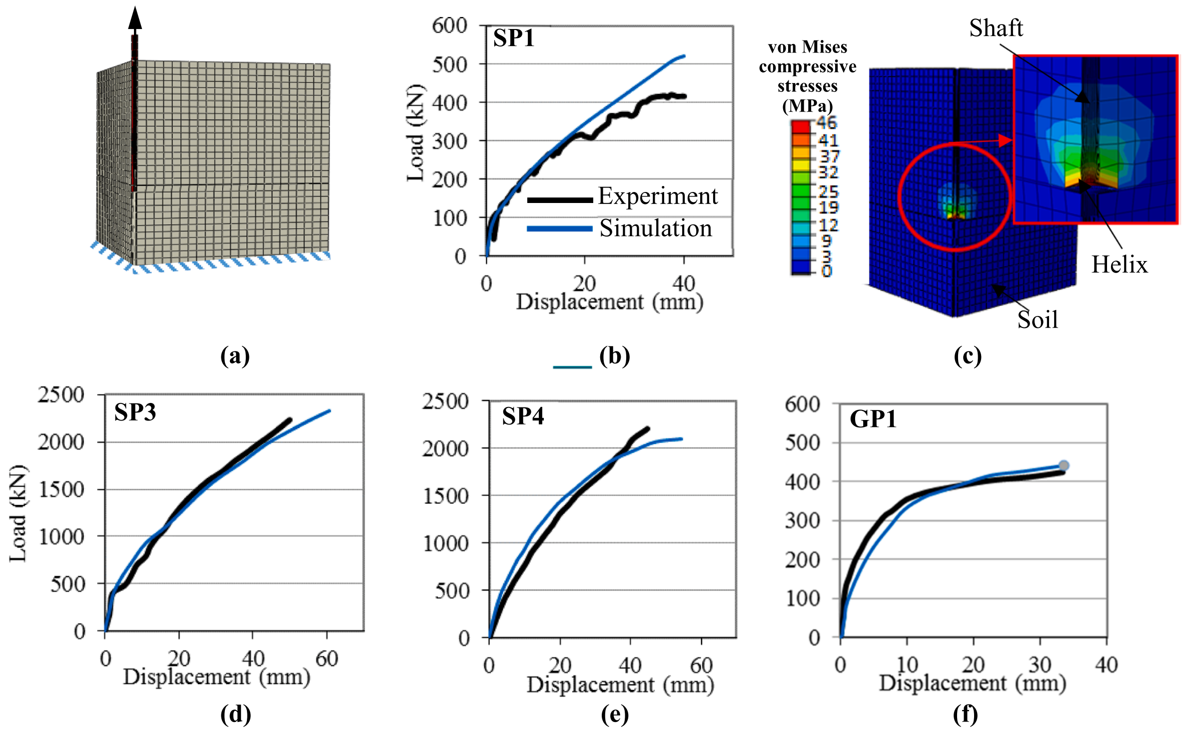

Fig. 11. (a) Discrete single pile and soil model, (b) load–displacement response, (c) soil stress distribution at failure, and the load–displacement responses for (d) SP3, (e) SP4, and (f) GP1.

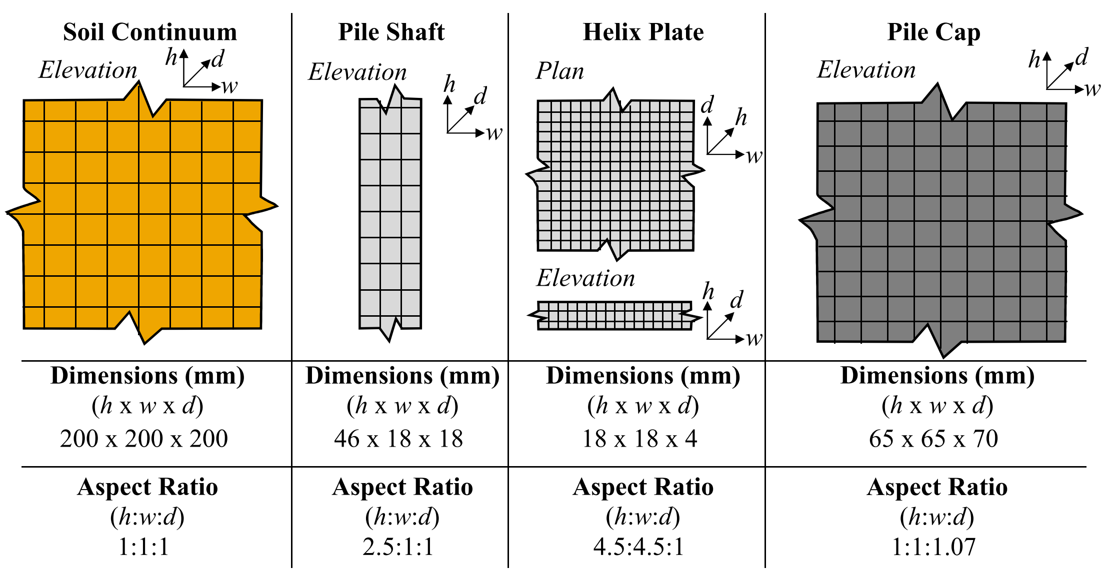

Fig. 12. Mesh distribution of the helical piles.

process. The simulated load–displacement responses and failure modes captured those of the experimental benchmarks (i.e., SP1, SP3, SP4, and GP1 in Fig. 6), as shown in Fig. 11. The von Mises stresses distribution of the helical pile group and soil model is used for predicting the load transfer and failure mechanisms (e.g., [3]), assuming the soil is under plastic yielding. The discrepancy between the FE simulation and experimental values of the peak load capacities is found to be less than 10%, indicating the successful calibration of the soil model.

In Stage 3, a system-level model is created, as shown in Fig. 7a. The experimentally calibrated material models for the concrete and soil, as obtained from Stages 1 and 2, are employed. The interaction between the soil and piles are modeled by a hard contact algorithm that minimizes the penetration of the soil surface into the pile (and vice-versa) while not allowing the transfer of tensile stresses normal to the

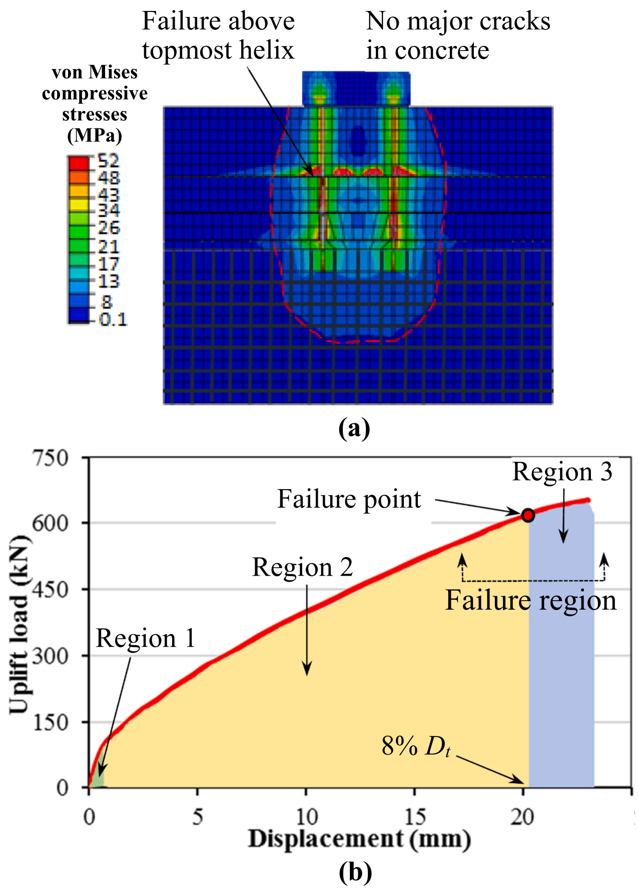

Fig. 13. (a) Stresses distribution at failure, and (b) system-level load–displacement response.

interface. The tangential behavior is dictated by a friction contact algorithm with a coefficient of friction (μ_{sp}) of 0.2. Similarly, the interaction between the soil and pile cap is modeled by a hard contact algorithm and a with a coefficient of friction (μ_{sc}) of 0.35 as per Table 4. The appropriate support conditions are applied and a displacement-controlled pushover analysis is performed for both the compression and uplift load cases.

A mesh sensitivity study is conducted to investigate the influence of the size of the elements used for the helical piles, soil, and pile cap. The mesh sizes of the soil and pile cap elements varied from coarse to intermediate, and fine meshes. The results obtained from the intermediate and fine meshes showed insignificant differences; consequently, the intermediate mesh (shown in Fig. 12a) is employed for computational efficiency. The mesh size of the helical pile, on the other hand, is found to have a significant influence on the system-level response; consequently, a fine mesh is used in the model. For the shaft elements, the mesh aspect ratio is kept below 3.0 (with the longer sides parallel to the shaft length) whereas for the helix plate elements, the mesh aspect ratio is defined as 1.0 for higher accuracy, as shown in Fig. 12. It is found that at least three elements are required through the thickness of the helix plate, where the strain gradient is higher, to better capture the stress distribution in the helix plates due to the soil bearing, as shown in Fig. 12.

The load–displacement response of the system, shown in Fig. 13b, can be divided into three distinct regions: the initial linear-elastic region with a high stiffness, the non-linear hardening region, and the plastic yielding and failure region, as shown in Fig. 13b. The first region represents the shaft friction while the second one represents the stress distribution to the soil surrounding the pile shaft and helices. The failure corresponding to 8% of the topmost helix diameter of 250 mm occurs at the transition from the second to third regions with an uplift capacity of 610 kN. The stress distribution in Fig. 13a demonstrates that the soil failure occurred above the topmost helix through the formation of a soil cone where the shear stress exceeds the shear strength of the soil, causing the soil element to fail above the topmost helix. The interface element between the concrete foundation and the soil contributes to the redistribution of the stresses, causing a reduction in the resisting forces at the ends of the piles and ultimately increasing the load and displacement capacities. The concrete foundation showed local cracking but did not fail, as the stresses were distributed uniformly on the interface between the foundation and the soil.

4. Comparisons with the discrete modeling approach

To demonstrate how the results from the traditional discrete modeling approach compare with those from the proposed system-level modeling methodology, the discrete pile cap and the discrete helical pile group and soil model are created, as shown in Fig. 14a and 14c. The results are examined in terms of the load capacities and the failure modes.

In the discrete pile cap model (see Fig. 14a and b), diagonal shear cracking occurred in the pile cap, which eventually led to the failure of concrete around the pile cap termination bracket. Hence, the uplift capacity of the discrete model was found to be 450 kN. In the discrete helical pile group and soil model (see Fig. 14c), the failure mode was in the soil above the topmost helix as shown in Fig. 14d, similar to the system-level model, with a capacity of 450 kN. Note that both system components are intentionally designed for the same load capacity to avoid an inconsistency due to the failure of the weaker component. The capacities obtained from these two discrete models are represented with horizontal lines in Fig. 15 and compared to the load–displacement response from the system-level model. The results show that the discrete models underestimate the load capacity by 26%. The load sharing and interaction between the system components permits the re-distribution of stresses, allowing for larger load and displacement capacities in the system-level model.

5. Influence of the soil type on the system-level response

To demonstrate the significance of the soil type, two more system-level models are created using organic clay (OL) and well-graded gravel soil (GW) with the properties shown in Table 7. Soil types are selected to represent conditions from soft to stiff, following the USCS soil classification.

The simulated load–displacement responses are presented in Fig. 16 along with the capacity lines obtained from the discrete models. The results indicate that stiffer soil not only significantly increases the capacity of the models but also reduces the discrepancy between the discrete and system-level models. This phenomenon can be attributed to the fact that, as the soil gets stiffer, the discrete modeling assumption of fixed or pinned piles becomes more realistic, thereby providing closer approximation to the system-level models.

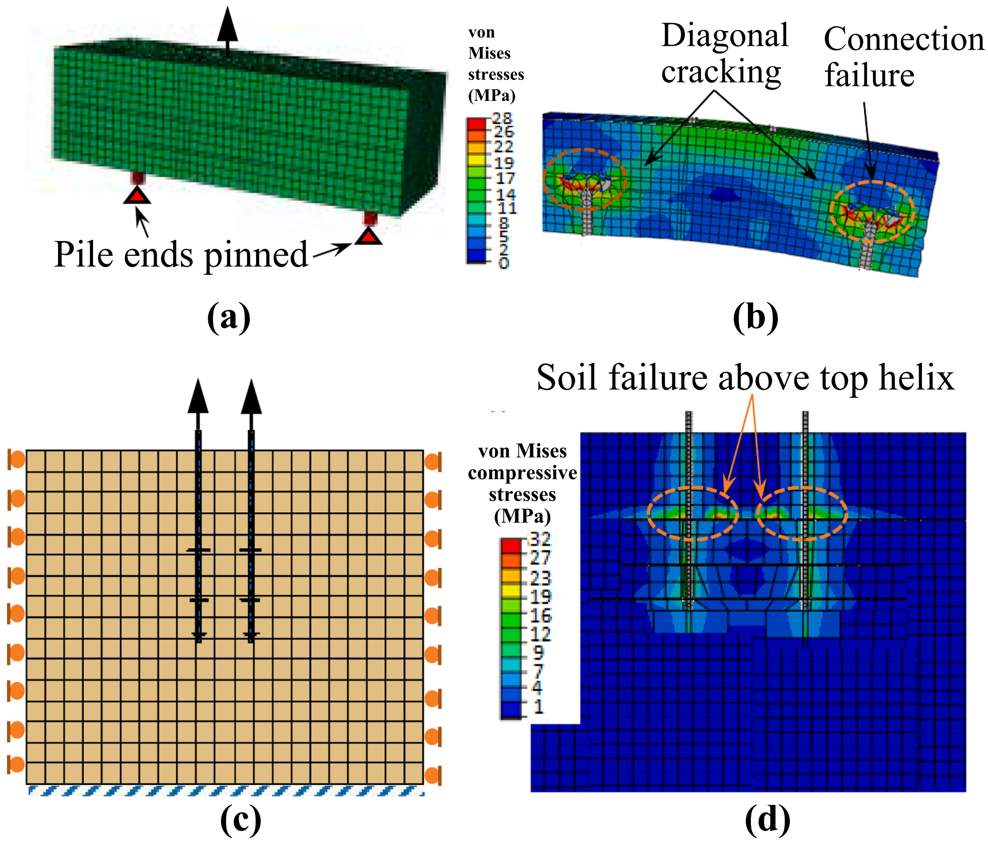

Fig. 14. (a) Discrete pile cap model, (b) deformations and stresses at failure, (c) discrete helical pile and soil model, and (d) soil stress at failure.

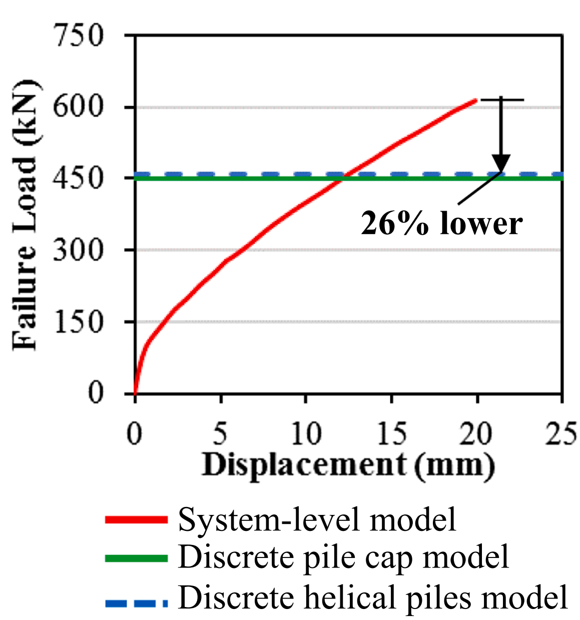

Fig. 15. Comparison of the discrete and system-level models (tensile load capacities).

Table 7
Soil parameters as per USCS [54].

USCS Soil-class	Description	*c* (kPa)	*Φ* (°)	Remarks
GW	Well-graded gravel	0	40	stiffer
GM-GL	Silty gravel	0	35	
OH	Organic clay, organic silt	10	22	soft

6. Influence of critical design parameters

To identify the design parameters critical for the uplift load performance, additional numerical studies are performed as discussed below.

6.1. Pile embedment into the pile cap

A system-level analysis is performed to estimate the ultimate capacities with different embedment depths of the helical pile termination brackets inside the pile cap. The simulations are performed in three embedment depth conditions inside the concrete pile cap as shown in Fig. 17a. The system-level uplift capacities obtained are plotted in Fig. 17b. The increase in the embedded depth inside the pile cap from bottom to middle increases the uplift capacity by 25%. This conclusion agrees well with the findings published in references [59,60]. By further increasing the embedment depth from the middle to the top, the uplift capacity only increases by 8%. The use of bottom embedment depth resulted in pre-mature cracking of concrete around the connection zone; the failure occurred in these zones by the detachment of the helical piles from the pile cap. Consequently, a middle embedment depth inside the pile cap is recommended considering both uplift and compression loads.

6.2. Pile embedment in the soil

Embedment depth is defined as the distance from the topmost helix plate to the ground surface. System-level models with three-helix piles are analyzed with soil embedment depths from 4000 mm to 5000 mm. The embedment in the concrete pile cap is fixed at 300 mm. The uplift capacities obtained are shown in Fig. 18a. The uplift capacity increases by 18% if the pile embedment in the soil is increased from 4000 mm to 4500 mm. On further increasing the embedment depth by 500 mm, the

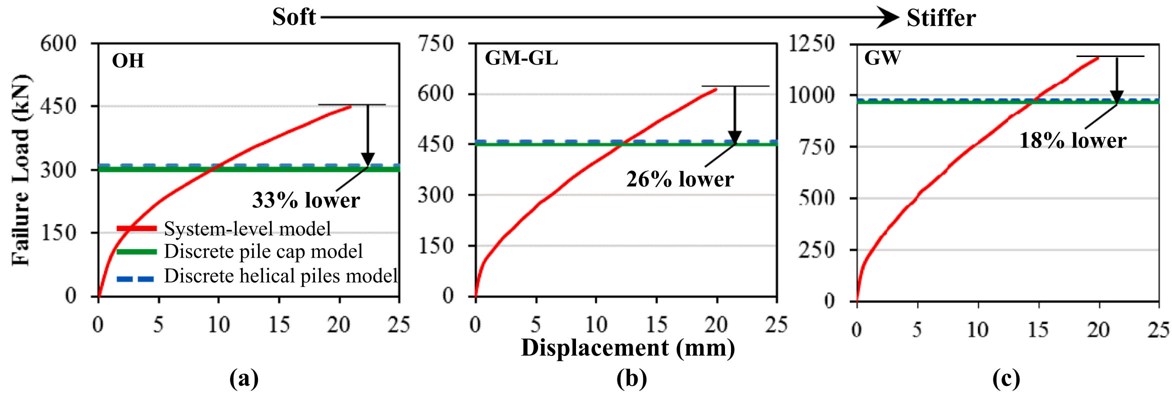

Fig. 16. Influence of different soil types on the three modeling approaches examined.

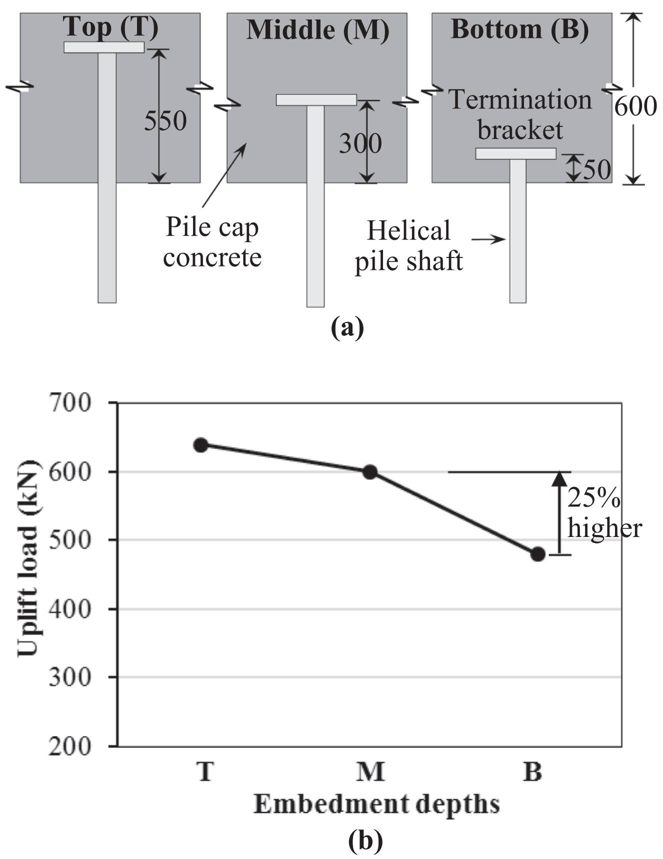

Fig. 17. (a) Embedment depths examined, and (b) variation of uplift capacities with the embedment depth.

capacity gain is similarly found to be 16%. With the increase in the pile embedment in the soil, the initial linear segment of the load–displacement curve becomes stiffer, which contributes to the increase in the capacity of the system.

6.3. Number of helices

The number of helices is varied from single to double and to triple. The load–displacement curves are shown in Fig. 18b. The uplift capacity of the pile is found to increase by 36% as the number of plates increases from single to double, where the soil between two helix plates act as a solid mass and provide extra capacity. By increasing the helix plate number from double to triple, the increase in the load capacity is found to be a smaller value of 18%.

7. Conclusions

A methodology is proposed for the system-level analysis of pile cap systems. The methodology can be applied to evaluate the static response of foundations on dry soils accounting for the material nonlinearities, and the interactions between the pile cap, helical pile group, and soil, using the experimentally verified failure mechanisms based on the relative displacement of the helical piles. The effectiveness of the methodology is demonstrated by comparing the results with the traditional discrete modeling approaches. In addition, the influences of the soil type, embedment depths, and number of helices on the holistic responses under uplift loads are investigated. The results from this study support the following conclusions:

- The traditional discrete modeling approaches have significant shortcomings in capturing the failure modes and the load capacities of the helical pile foundation systems. The influence of the soil is neglected during the structural pile cap modeling while the influence of the concrete pile cap is neglected during the helical pile and soil modeling.
- As compared to the system-level model, including all system components, the discrete modeling approach underestimated the load capacities by up to 33% under uplift for the systems considered in this study. The largest discrepancy is obtained for softer soils.
- The load capacity predictions from the discrete and system-level modeling approaches converge as the soil becomes stiffer because the discrete modeling assumption of fixed or pinned boundary conditions become more realistic in stiffer soils.
- The system-level models demonstrate that the location of the helical pile termination bracket inside the concrete pile cap has a significant influence on the uplift capacity of the entire system. The bottom embedment depth resulted in failures at load capacities that were 25% less than those obtained from the middle embedment depths. In addition, the bottom embedment depth resulted in premature concrete cracking at the connection zone – a concern for long-term durability.
- A well-defined 3D modeling methodology is proposed to better understand the holistic behavior of helical pile foundation systems and more accurately quantify their load and displacement responses and failure modes, including the premature and undesirable ones involving connection zones.
- The proposed methodology uses experimentally calibrated material models without requiring the use of any specific computer program on the condition that the program used can capture the significant failure mechanisms demonstrated in this study. Experimental benchmark sets and how the calibration process is conducted is defined in detail in this study.
- The studies conducted demonstrate the suitability of using a failure criterion based on a displacement equivalent to 8% of the topmost

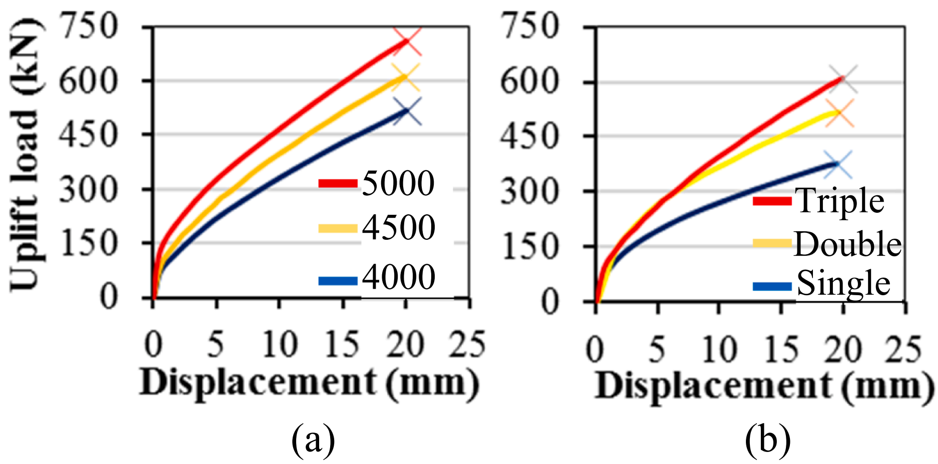

Fig. 18. Influence of: (a) the pile embedment inside the soil, and (b) the number of helices on the uplift load capacity.

helix plate diameter. This finding is also supported by the experimental evidence available in the literature.
– The system-level modeling results demonstrate that higher load capacities are obtained with the increase in the number of helices, the pile embedment depths inside the soil, and the termination plate embedment inside the concrete pile cap.

Appendix A. Supplementary material

Supplementary data to this article can be found online at https://doi.org/10.1016/j.engstruct.2020.110977.

References

[1] Perko HA. Helical piles: A practical guide to design and installation. New Jersey: John Wiley & Sons, Inc; 2009, 512 pp. https://doi.org/10.1002/9780470549063.ch12.
[2] Mohajerani A, Bosnjak D, Bromwich D. Analysis and design methods of screw piles: a review. Soils Found 2016;56(1):115–28. https://doi.org/10.1016/j.sandf.2016.01.009.
[3] Kwon O, Lee J, Kim G, Kim I, Lee J. Investigation of pullout load capacity for helical anchors subjected to inclined loading conditions using coupled Eulerian-Lagrangian analyses. Comput Geotech 2019;111:66–75. https://doi.org/10.1016/j.compgeo.2019.03.007.
[4] Guner S, Carrière J. Analysis and strengthening of caisson foundations for uplift loads. Can J Civ Eng 2016;43(5):411–9http://www.utoledo.edu/engineering/faculty/serhan-guner/docs/JP6_Guner_Carriere_2016.pdf.
[5] Young JJM. Uplift capacity and displacement of helical anchors in cohesive soil. MS Thesis, School of Civil and Construction Engineering, Oregon State University; 2012, 156 pp. https://ir.library.oregonstate.edu/downloads/j6731765j.
[6] Fahmy A, El Naggar MH. Axial performance of helical tapered piles in sand. Geotech Geol Eng 2017;35(4):1549–76. https://doi.org/10.1007/s10706-017-0192-1.
[7] Sakr M. Installation and performance characteristics of high capacity helical piles in cohesionless soils. DFI Journal, The Journal of the Deep Foundations Institute 2011;5(1):39–57. https://doi.org/10.1179/dfi.2011.004.
[8] Haldar S, Basu D. Response of Euler-Bernoulli beam on spatially random elastic soil. Computer and Geotechnics 2013;50:110–28. https://doi.org/10.1016/j.compgeo.2013.01.002.
[9] Mendoza CC, Cunha R, Lizcano A. Mechanical and numerical behavior of group of screw (type) piles founded in a tropical soil of the Midwestern Brazil. Computer and Geotechnics 2015;67:187–203. https://doi.org/10.1016/j.compgeo.2014.09.010.
[10] Meléndez C, Miguel PF, Pallarés L. A simplified approach for the ultimate limit state analysis of three-dimensional reinforced concrete elements. Eng Struct 2016;123:330–40. https://doi.org/10.1016/j.engstruct.2016.05.039.
[11] Uffe G, Jensen UG, Hoang LC. Collapse mechanisms and strength prediction of reinforced concrete pile caps. Eng Struct 2012;35:203–14. https://doi.org/10.1016/j.engstruct.2011.11.006.
[12] ASCE/SEI 7-16. Minimum design loads and associated criteria for buildings and other structures. Reston, VA, USA: American Society of Civil Engineers. 2017, 800 pp.
[13] Hu L, Pu JL. Application of damage model for soil–structure interface. Comput Geotech 2003;30(2):165–83. https://doi.org/10.1016/S0266-352X(02)00059-9.
[14] Chen L, Poulos HG. Analysis of pile-soil interaction under lateral loading using infinite and finite elements. Comput Geotech 1993;15(4):189–220. https://doi.org/10.1016/0266-352X(93)90001-N.
[15] EN 1997-1:2014. Eurocode 7: Geotechnical Design - Part 1: General Rules; German Version EN 1997-1:2004 + AC:2009 + A1:2013. Brussels, Belgium: Standardization European Committee. 2014, 175 pp.
[16] Cao J. The shear behaviour of the reinforced concrete four-pile caps. Ph.D. Thesis, School of Civil Engineering and the Environment, University of Southampton, Southampton, UK, 2009, 287 pp. https://eprints.soton.ac.uk/73699/.
[17] Suzuki K, Otsuki K. Experimental study on corner shear failure of pile caps. Trans Jpn Concr Inst 2002;23:303–10https://ci.nii.ac.jp/naid/10007251043/.
[18] Suzuki K, Otsuki K, Tsubata T. Influence of edge distance on failure mechanism of pile caps. Trans Jpn Concr Inst 2000;22:361–7https://ci.nii.ac.jp/naid/10007467724/.
[19] Elsherbiny ZH, El Naggar MH. Axial compressive capacity of helical piles from field tests and numerical study. Can Geotech J 2013;50(12):1191–203. https://doi.org/10.1139/cgj-2012-0487.
[20] Oliver YP. Comparison of finite difference and finite volume methods & the development of an education tool for the fixed-bed gas adsorption problem. Ph.D. Dissertation, Department of Chemical and Biomolecular Engineering, National University of Singapore, Singapore; 2011, 67 pp.
[21] Peiró J, Sherwin S. Finite difference, finite element and finite volume methods for partial differential equations. Handbook of Materials Modeling 2005:2415–46.
[22] Labuz JF, Zang A. Mohr-Coulomb failure criterion. Rock Mech Rock Eng 2012;45(6):975–9https://link.springer.com/article/10.1007/s00603-012-0281-7.
[23] Alejano LR, Bobet A. Drucker-Prager criterion. Rock Mech Rock Eng 2012;45:995–9https://link.springer.com/article/10.1007/s00603-012-0278-2.
[24] Krenk S. Characteristic state plasticity for granular materials, Part 1: Basic theory. Int J Solids Struct 2000;37:6343–60https://www.sciencedirect.com/science/article/pii/S0020768399002784.
[25] Rawat S, Gupta AK. Numerical modelling of pullout of helical soil nail. J Rock Mech Geotech Eng 2017;9(4):648–58. https://doi.org/10.1016/j.jrmge.2017.01.007.
[26] Salhi L, Nait-Rabah O, Deyrat C, Roos C. Numerical modeling of single helical pile behavior under compressive loading in sand. EJGE 2013;18:4319–38http://www.ejge.com/2013/Ppr2013.395mlr.pdf.
[27] Tan SA, Ooi PH, Park TS, Cheang WL. Rapid pullout test of soil nail. J Geotech Environ Eng 2008;134(9):1327–38. https://doi.org/10.1061/(ASCE)1090-0241(2008)134:9(1327).
[28] Dib M, Kouloughli S, Hecini M. Numerical analysis of high capacity helical piles subjected to ground movement in weathered unstable clayey slope. Comput Geotech 2019;110:319–25. https://doi.org/10.1016/j.compgeo.2019.01.024.
[29] George BE, Banerjee S, Gandhi SR. Numerical analysis of helical piles in cohesionless soil. Int J Geotech Eng 2017:1–15. https://doi.org/10.1080/19386362.2017.1419912.
[30] Van Baars S, Van Niekerk WJ. Numerical modelling of tension piles. In: International Symposium on Beyond 2000 in Computational Geotechnics 1999; 237–246.
[31] Mroueh H, Shahrour I. Numerical analysis of the response of battered piles to inclined pullout loads. Int J Numer Anal Meth Geomech 2009;33(10):1277–88.
[32] Tamayo JL, Awruch AM. On the validation of a numerical model for the analysis of soil-structure interaction problems. Latin American Journal of Solids and Structures. 2016;13(8):1545–75.
[33] Kranthikumar A, Sawant VA, Shukla SK. Numerical modeling of granular anchor pile system in loose sandy soil subjected to uplift loading. Int J Geosynthetics Ground Eng 2016;2(2):15 pp.
[34] Zhou WH, Yin JH, Hong CY. Finite element modelling of pullout testing on a soil nail in a pullout box under different overburden and grouting pressures. Can Geotech J 2011;48(4):557–67. https://doi.org/10.1139/t10-086.
[35] Livneh B, El Naggar MH. Axial testing and numerical modeling of square shaft helical piles under compressive and tensile loading. Can Geotech J 2008;45(8):1142–55. https://doi.org/10.1139/T08-044.
[36] Cerato A, Victor R. Effects of long-term dynamic loading and fluctuating water table on helical anchor performance for small wind tower foundations. J Perform Constr Facil 2009;23(4):251–61. https://doi.org/10.1061/(ASCE)CF.1943-5509.0000013.
[37] Lee J, Fenves GL. Plastic-damage model for cyclic loading of concrete structures. J Eng Mech 1998;124(8):892–900. https://doi.org/10.1061/(ASCE)0733-

9399(1998)124:8(892).
[38] Lubliner J, Oliver J, Oller S, Oñate E. A plastic-damage model for concrete. Int J Solids Struct 1989;25(3):299–326. https://doi.org/10.1016/0020-7683(89)90050-4.
[39] Das BM. Shallow foundations: bearing capacity and foundation. CRC Press 2017;400:pp. https://doi.org/10.1201/9781315163871.
[40] ACI Committee 318. Building code requirements for structural concrete (ACI 318-19) and Commentary. Farmington Hills, MI, USA: American Concrete Institute. 2019, 623 pp.
[41] Vecchio FJ, Shim W. Experimental and analytical reexamination of classic concrete beam tests. J Struct Eng ASCE 2004;130(3):460–9http://www.vectoranalysisgroup.com/journal_publications/jp49.pdf.
[42] Diab MAM. Behavior of helical pile connectors for new foundations. Ph.D. Dissertation, School of Civil and Environment Engineering, University of Western Ontario, London, Ontario, Canada; 2015, 638 pp. https://ir.lib.uwo.ca/cgi/viewcontent.cgi?article=4736&context=etd.
[43] Sun DA, Yao YP, Matsuoka H. Modification of critical state models by Mohr-Coulomb criterion. Mech Res Commun 2006;33(2):217–32. https://doi.org/10.1016/j.mechrescom.2005.05.006.
[44] Popa HO, Batali LO. Using Finite Element Method in geotechnical design. Soil constitutive laws and calibration of the parameters. Retaining wall case study. WSEAS Trans Appl Theor Mech 2010;5(3):177–86.
[45] David T, Krishnamoorthy R, Cahyadi BI. Finite element modelling of soil-structure interaction. J Teknol. 2015;76:59–63.
[46] Brinkgreve RB, Swolfs WM, Engin E, Waterman D, Chesaru A, Bonnier PG, Galavi V. PLAXIS 2D 2010. User manual 2010.
[47] Noor ST, Hanna A, Mashhour I. Numerical modeling of piles in collapsible soil subjected to inundation. Int J Geomech 2013;13(5):514–26.
[48] Lutenegger AJ. Quick design guide for screw-piles and helical anchors in soils. International Society for Helical Foundations 2015;13:pp.
[49] Department of the Navy Naval Facilities Engineering Command, Foundations and Earth Structures, NAVFAC Design Manual 7.2; 1982.
[50] Pack JS. Practical design and inspection guide for helical piles and helical tension anchors. IMR, Inc., Denver, Colorado; 2009, 194 pp.
[51] Gavin K, Doherty P, Tolooiyan A. Field investigation of the axial resistance of helical piles in dense sand. Can Geotech J 2014;51(11):1343–54. https://doi.org/10.1139/cgj-2012-0463.
[52] Sakr M. Comparison between high strain dynamic and static load tests of helical piles in cohesive soils. Soil Dyn Earthquake Eng 2013;54:20–30. https://doi.org/10.1016/j.soildyn.2013.07.010.
[53] Lanyi-Bennett SA, Deng L. Axial load testing of helical pile groups in a glaciolacustrine clay. Can Geotech J 2018;56(2):187–97https://www.nrcresearchpress.com/doi/pdfplus/10.1139/cgj-2017-0425.
[54] Howard AK. The revisited ASTM standard on the unified classification system. Geotech Test J 1984;7(4):216–22. https://doi.org/10.1520/GTJ10505J.
[55] Luo C, Yang X, Zhan C, Jin X, Ding Z. Nonlinear 3D finite element analysis of soil–pile–structure interaction system subjected to horizontal earthquake excitation. Soil Dyn Earthquake Eng 2016;84:145–56.
[56] Ghaly AM, Clemence SP. Pullout performance of inclined helical screw anchors in sand. J Geotech Geoenviron Eng 1998;124(7):617–27.
[57] ABAQUS v6.14. Analysis user's guide. Vol. IV, Dassault Systemes, Providence, Rhode Island, 2014; 1098 pp. http://130.1.49.89.49:2080/v6.14/index.html.
[58] Li W, Deng L. Axial load tests and numerical modeling of single-helix piles in cohesive and cohesionless soils. Acta Geotech 2019;14(2):461–75.
[59] Guner S, Chiluwal S. Cyclic load behavior of helical pile-to-pile cap connections subjected to uplift forces. Engineering Structures 2019 (submitted) http://www.utoledo.edu/engineering/faculty/serhan-guner/docs/Guner_Chiluwal_Helical_Pile_Connections_Submitted.pdf.
[60] Chiluwal S, Guner S. Design recommendations for helical pile anchorages subjected to cyclic load reversals," Final Project Report, Deep Foundation Institute, Hawthorne NJ, USA; 2019; 173 pp. http://www.utoledo.edu/engineering/faculty/serhan-guner/docs/R2_DFI_Helical_Pile_Anchorages.pdf.